Ferromagnetic Resonance Spectroscopy of CoFeZr-CaF$_2$ Granular Nanocomposites

Tomasz N. Kołtunowicz[1, *], Vitalii Bondariev[2], Pawel Zukowski[1], Julia Sidorenko[2], Vadim Bayev[3], and Julia A. Fedotova[3]

Abstract—Results of the study of magnetic properties of nanocomposite samples $(\text{CoFeZr})_x(\text{CaF}_2)_{(100-x)}$ (31 at.% $\leq x \leq$ 47 at.%) produced in argon (Ar) and argon with oxygen (Ar with O$_2$) sputtering atmosphere are presented in this paper. The magnetic resonance spectroscopy at room temperature using continuous wave X-band electron spin resonance (ESR) was used for analysis of samples magnetic properties. After analysis it is established that in the case of samples produced in argonsputtering atmosphere the value of g increases with the rise of metal content and for samples produced in argon with oxygen atmosphere the value g decrease with the rise of x. Such a behavior of $g(x)$ is explained by the presence of core-shell structure of NPs represented by ferromagnetic core and antiferromagnetic core that results in quenching of orbital motion of electrons.

1. INTRODUCTION

High interest in nanostructured materials, which in their composition contain nanoparticles, nanotubes, layers, and nanograins, is due to their unique properties [1–3]. Nanoparticles of the magnetic materials, whose size is comparable to or smaller than the magnetic domain of the massive sample, demonstrate the greatest interest (for example, ferromagnetic alloys). Such particles can have a much higher magnetic anisotropy than massive materials [4], magnetization per atom, etc. [5–7].

Metal-dielectric nanocomposites exhibit physical properties that differ from the properties of single-phase materials, including nanogranular materials. By changing the concentration of the metallic phase (x) it is possible to significantly change magnetic and electrical properties and change nanocomposite parameters from matrix properties to filler properties. So in composites with a small value x, metallic particles are isolated from each other. Superparamagnetic properties are characteristic for them [8–11], and materials with such composition exhibit a high magneto resistive effect [9, 11, 12]. With the increase of the metallic particles concentration, and hence with the reduction of the distance between them, their magnetic interactions begin to appear.

The use of nanoparticles of FeCo alloy in nanocomposites results in low magnetic coercivity and high magnetization of the materials, which, with high resistivity and tunnel negative magneto resistance, allows them to be used in the development of different magnetoelectronic devices, in particular, magnetic field sensors for high frequency applications. The development of systems with high anisotropy of nanoparticles and respectively increased magnetic coercion allows them to be used to develop high density data storage media [13, 14], and to develop devices for visualizing the magnetic field [15, 16].

The aim of this study was to investigate the magnetic properties of nanocomposites with the $(\text{FeCoZr})_x(\text{CaF}_2)_{(100-x)}$ structure with a metallic phase content below the percolation threshold x_c produced by sputtering a target consisting of a CoFeZr alloy and a CaF$_2$ dielectric with an argon (Ar) ion beam and determining the effect of presence of oxygen in the sputtering beam for these properties.

2. METHODS AND EXPERIMENTAL RESULTS

To obtain the tested nanogranular composite layers $(FeCoZr)_x(CaF_2)_{(100-x)}$ the ion-beam sputtering method was used [17, 18]. The sputtered target used to make nanocomposites consisted of a metallic plate $270 \times 70 \times 14$ mm from $Fe_{45}Co_{45}Zr_{10}$ alloy, on which CaF_2 dielectric strips were attached. The alloy was prepared from especially pure carbonyl iron (99.90%), especially pure cobalt (99.98%) and zirconium (99.80%). CaF_2 dielectric strips about 2 mm thick and 9 mm wide were attached to the alloy plate at different distances from each other (from 3 mm on one edge to 24 mm on the other). The target was sputtered in a vacuum chamber and the sputtered material deposited on the glass-ceramic dielectric substrate. The target material was sputtered in the argon (Ar) or mixed argon with oxygen (Ar with O_2) atmospheres. The substrate was placed on the inner surface of the drum, which rotated at an adjustable frequency in the range of 0.001 to 1 rpm. The positive potential that appears on the surface of the dielectric was neutralized by means of a compensator — a source of electron radiation.

The components of the composite target (FeCoZr and CaF_2 alloy) have very different surface energy values, $2.5 \, J/m^2$ and $0.45 \, J/m^2$ respectively [19]. When these two components were sprayed, they deposited on the substrate simultaneously. By diffusing on the substrate, dielectric atoms focused around the metal alloy atoms. In this way, phase atoms with a high surface energy value (metallic alloy) formed spherical grains in a dielectric matrix (low surface energy phase). In this way, a layer of nanocomposite about 1 µm thick was deposited on a glass-ceramic substrate about 1 mm thick. Two series of nanocomposite $(FeCoZr)_x(CaF_2)_{(100-x)}$ samples were produced in Ar ($P_{Ar} = 110$ mPa) and Ar with O_2 ($P_{Ar} = 90$ mPa, $P_O = 9.8$ mPa) sputtering atmospheres. Samples with a metallic phase content of 31 at.% $\leq x \leq$ 47 at.% were selected for testing, i.e., with a metallic phase content below the percolation threshold $x_c \approx 50$ at%. It was caused by the fact that there is metallic conduction above the percolation threshold. The analysis of the sample composition was made by the method of energy-dispersion X-ray microanalysis (EDX) using a scanning electronic microscope JSM-5610 LV equipped with the chemical analysis system EDX JED-2201 from JEOL (Japan). Studies on the structure of nanocomposites were carried out immediately after the production of nanocomposites.

Figure 1 shows pictures of Transmission Electron Microscopy (TEM) of nanocomposite $(FeCoZr)_x(CaF_2)_{(100-x)}$ with the content of metallic phase $x = 39$ at.% produced by pure argon ion beam sputtering. The distribution of dimensions of nanoparticles is similar to the Gaussian distribution — shown by a continuous line. The analysis of the size of the metallic phase nanoparticles (Figure 1) showed that their average size was 3.3 nm, and the standard deviation was 0.2 nm. The sizes of nanoparticles range from about 1.5 nm to 6.5 nm. It can be seen from the electronogram that the layer formed by sputtering with the Ar beam consists of grains of the FeCoZr metallic phase placed in the CaF_2 dielectric matrix (insert in Figure 1). It follows that the elements of the metallic alloy and dielectric matrix do not form chemical compounds with each other.
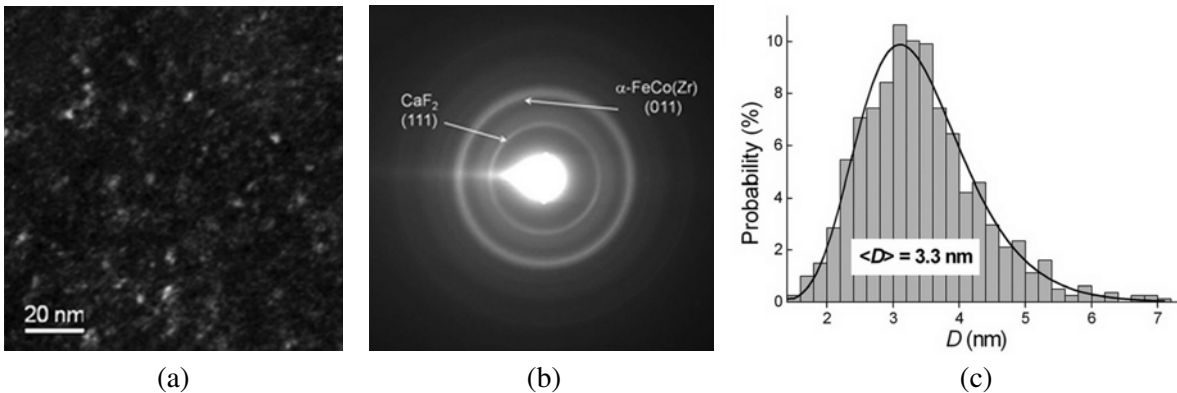

(a) (b) (c)

Figure 1. Plan-view transmission electron microscopy analysis of nanocomposite $(FeCoZr)_{39}(CaF_2)_{61}$ produced by sputtering in pure argonatmosphere: (a) dark-field image; (b) SAED pattern taken from a large surface area; (c) evaluated size distribution of the metallic nanograins [20].
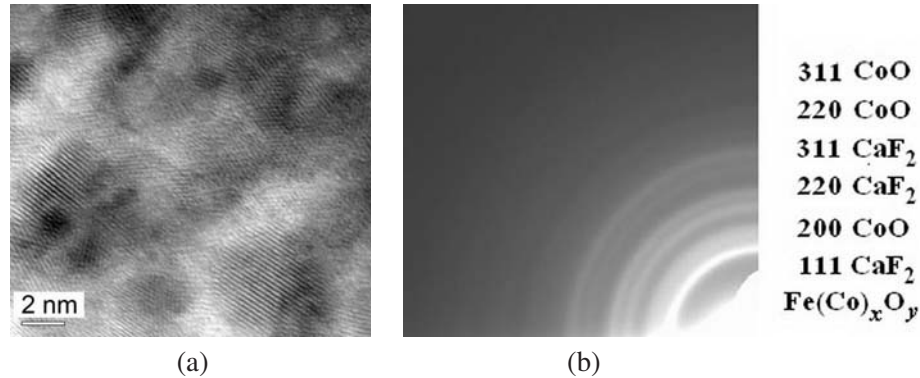
(a)   (b)

Figure 2. (a) High resolution transmission electron microscopy and (b) electronogram of nanocomposite $(FeCoZr)_{38}(CaF_2)_{62}$ produced by sputtering in mixed (Ar with O_2) atmosphere.

Figure 2(a) shows the image of the nanocomposite $(FeCoZr)_x(CaF_2)_{(100-x)}$ with the content of the metallic phase $x = 38$ at.% made using High Resolution Transmission Electron Microscopy (HRTEM). The figure shows that the nanoparticles have dimensions of about 6–8 nm. The layer electronogram is shown in Figure 2(b). It shows that the use of mixed (Ar with O_2) atmosphere led to complete oxidation of the metallic phase atoms with the formation of crystalline CoO and $Fe(Co)_xO_y$ phases [21].

Magnetic properties of $(CoFeZr)_x(CaF_2)_{(100-x)}$ (31 at.% $\leq x \leq$ 47 at.%) nanocomposite films (produced inArandAr with O_2 sputtering atmosphere) were analyzed by magnetic resonance spectroscopy at room temperature using continuous wave X-band (microwave frequency 9.32 GHz) electron spin resonance (ESR) spectrometer Varian E112 with modulation of magnetic field at frequency 100 kHz (the absorption signal is detected as its first derivative in the spectrum) [22]. To reveal magnetic anisotropy peculiarities of the samples, angular dependence of the induction of resonance field (B_r) was measured and analyzed.

The orientation of samples in an external magnetic field was characterized by the polar angle θ_B (an angle between the normal vector of sample surface and the vector of magnetic induction of external field B) and by the azimuth ϕ [23, 24]. The θ_B value of 0° corresponds to the direction of external magnetic field perpendicular to the surface of a sample — out-of-plane (OOP). Similarly, the direction of external magnetic field is parallel to the surface of a sample ($\theta_B = 90°$) — in-plane (IP). The features of magnetic anisotropy were characterized in terms of demagnetizing field B_d.

Typical magnetic resonance spectra of $(CoFeZr)_x(CaF_2)_{(100-x)}$ films at different orientations in external magnetic field are exemplified in Figure 3 illustrating spectra of $(CoFeZr)_{47}(CaF_2)_{53}$ samples produced in Ar and Ar with O_2 sputtering atmospheres. Spectra signals represent wide intense single

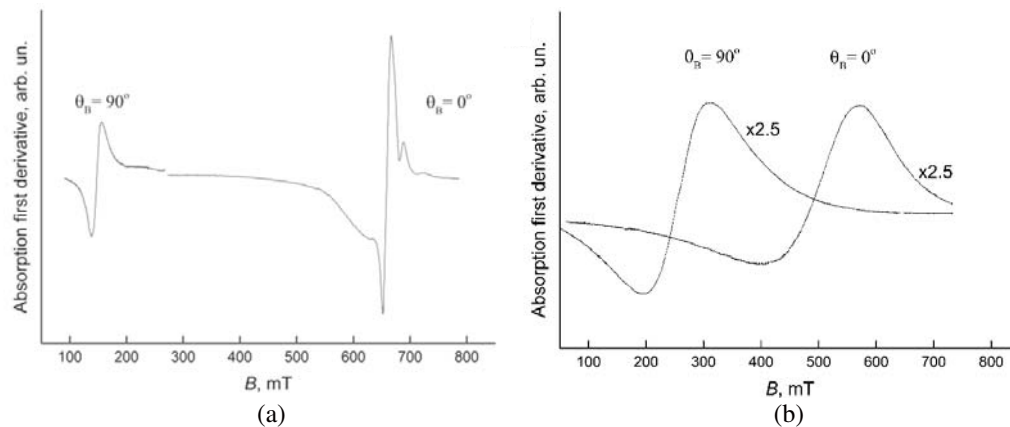(a)   (b)

Figure 3. Magnetic resonance spectra of film $(CoFeZr)_{47}(CaF_2)_{53}$ produced in (a) Ar and (b) Ar with O_2 sputtering atmosphere at different sample orientations in external magnetic field.

lines with B_r values strongly depending on angle θ_B (as an example an angle dependence $B_r(\theta)$ for $(CoFeZr)_{47}(CaF_2)_{53}$ sample produced in argon sputtering atmosphere is illustrated on Figure 5). Specified signals are not saturated with microwave power increase. These features of magnetic resonance spectra of nanocomposite film indicate that resonance absorption has a ferromagnetic nature. Also for samples produced in argon sputtering atmosphere with $x \geq 34.1$ at.% spin wave resonance (SWR) lines were observed at out-of-plane orientation of the sample. It should be noted that in a case of in-plane orientation of the samples in the external magnetic field the value B_r does not depend on the angle ϕ, evidencing isotropic magnetic properties in the film's plane.

The values of g-factor (g) and induction of demagnetizing field B_d were determined using the dependence of B_r value on the angle θ_B between induction B and normal n [23] in assumption of uniform CoFeZr NPs distribution in CaF_2 matrix and homogeneous magnetization of metal nanoparticles (NPs). A quite homogeneous distribution of quasi-spherical FeCoZr NPs inside CaF_2 matrix at $x \leq 50$ is clearly confirmed by transmission electron microscopy images presented in [25–27], while homogeneous magnetization of NPs is presumed by their small medium diameter within single-domain limit [25–28].

Table 1 summarizes the values of B_r for all studied films at various θ_B that were used for calculations of g and B_d values.

Table 1. Values of B_r of nanocomposites produced in argon (Ar) and argon with oxygen (Ar with O_2) sputtering atmosphere at different film's orientations in external magnetic field.

	Metal content x in granular films, at.%							
	produced in Ar sputtering atmosphere				produced in Ar with O_2 sputtering atmosphere			
	31	34	42	47	31	34	42	47
$B_r(\theta_B = 0°)$, mT	530	556	572	659	372.9	351	419	481
$B_r(\theta_B = 90°)$, mT	207	191	164	148	269	281	261	250

Using the energy dispersion relationship and Landau-Lifshitz magnetization dynamics model for a classic mode of FMR spectra registration (microwave frequency is constant and B changes linearly with time) the resonance frequency is determined by the following expression [29]:

$$(hf/g\mu_B)^2 = [B_r\text{Cos}(\theta_B - \theta_M) + B_d\text{Cos}(2\theta_M)][B_r\text{Cos}(\theta_B - \theta_M) + B_d\text{Cos}^2(\theta_M)], \quad (1)$$

where: h — Planck constant, f — microwave frequency, μ_B — Bohr magneton, B_d — induction of demagnetizing field. In Eq. (1), B_d is defined as $B_d = (N_{IP} — N_{OOP}) \cdot \mu_0 \cdot M$, where N_{IP} and N_{OOP} — demagnetizing factors of the sample towards in-plane and out-of-plane directions correspondingly, μ_0 — vacuum permeability, M — sample magnetization. The angle between magnetization M and normal n (θ_M) is defined by the condition of minimum of free energy density of the system:

$$B \cdot \text{Sin}(\theta_B - \theta_M) + B_d \cdot \text{Sin}(2\theta_M) = 0. \quad (2)$$

Assuming isotropic magnetization of samples in the plane of films values of g-factor and B_d of $(CoFeZr)_x(CaF_2)_{(100-x)}$ (31 at.% $\leq x \leq$ 47 at.%) nanocomposites are determined considering values of B_r at two orientations: $\theta_B = 0°$ and $\theta_B = 90°$ (B_{OOP} and B_{IP}, respectively). For the case of films uniformly magnetized with the value of induction close to magnetic saturation we can presume that $\theta_{IP} \to 0°$ and $\theta_{OOP} \to 90°$. Thus using Equations (1) and (2), the following system of equations for each sample is obtained:

$$\begin{cases} \left(\dfrac{hf}{g\mu_B}\right)^2 = (B_{OOP} - B_d)^2, \\ \left(\dfrac{hf}{g\mu_B}\right)^2 = B_{IP}(B_{IP} + B_d). \end{cases} \quad (3)$$

The sign of B_d indicates the magnetic anisotropy type of a sample. A positive value of B_d is associated with an easy axis type of magnetic anisotropy (the axis of easy magnetization is directed perpendicular towards the film surface), while negative value of B_d is a signature of an easy plane type of
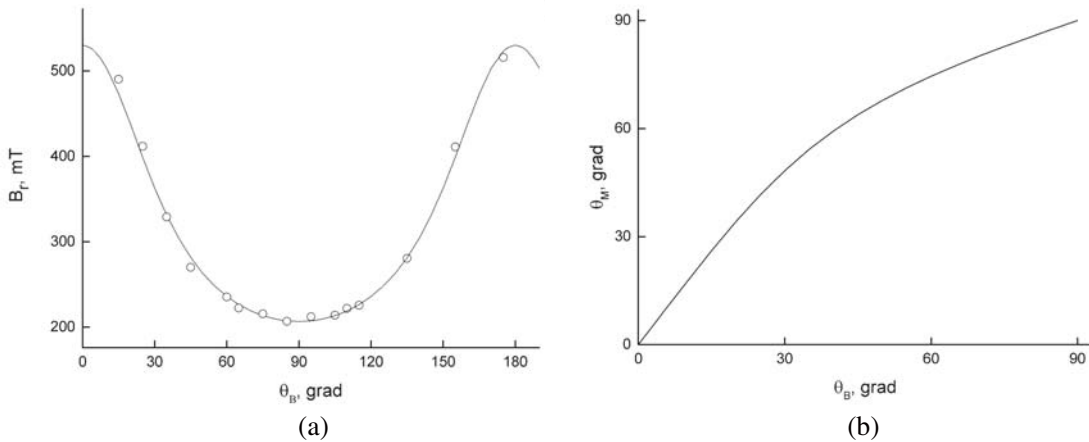
Figure 4. Experimental (pointed by circles) and calculated (pointed by line) angular dependences of the induction of resonance magnetic field $B_r(\theta_B)$ for the $(CoFeZr)_{31}(CaF_2)_{69}$ film produced in Ar atmosphere (a) and theoretically calculated dependence of angle between magnetization M and normal n (θ_M) on angle between induction of external magnetic field B and normal n (θ_B) used for calculations of angular dependence $B_r(\theta_B)$ (b).

magnetic anisotropy (the plane of easy magnetization coincides with the surface of film) [28, 29]. Using the values of g and B_d for Equations (1) and (2), we calculated the theoretical dependences of $B_r(\theta_B)$ and $\theta_M(\theta_B)$ for the film $(CoFeZr)_{31}(CaF_2)_{69}$ as represented in Figures 4(a) and 4(b), respectively.

As one can see theoretical dependence of $B_r(\theta_B)$ is in a very good agreement with experimental data that indicates an applicability of chosen mathematic model (see Figure 4(a)). A good agreement of experimental data with theoretical calculations was observed for all the samples.

3. DISCUSSION

Values of g for granular films $(CoFeZr)_x(CaF_2)_{(100-x)}$ $(31$ at.% $\le x \le 47$ at.%$)$ produced in argon and argon with oxygen sputtering atmosphere calculated using Eq. (3) are shown in Figure 5. It is seen that the dependences of g-factor on x of samples produced in Ar and Ar with O_2 sputtering atmosphere differ in essence. In the case of samples produced in Ar sputtering atmosphere the value of g increases with the rise of metal content, while for samples produced in Ar with O_2 sputtering atmosphere the value of g decreases with the rise of x. A similar behavior of $g(x)$ is observed for CoFeZr NPs in Al_2O_3
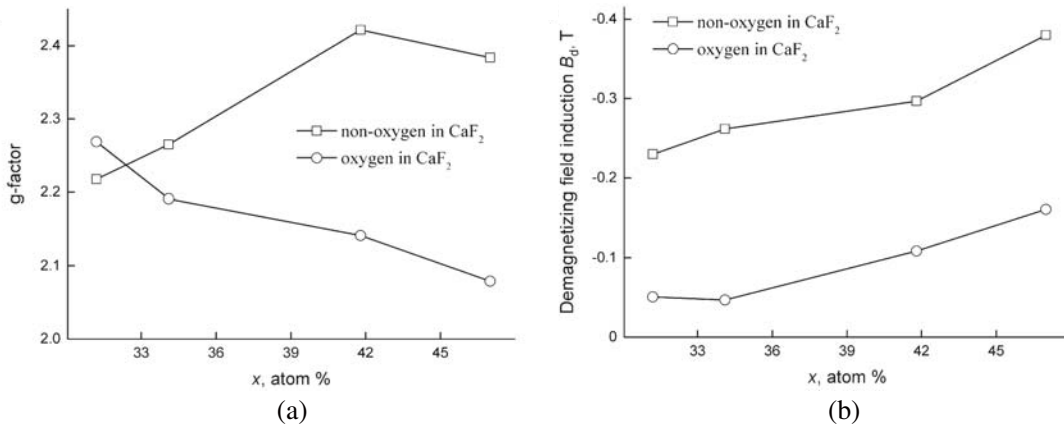

Figure 5. (a) The dependence of g-factor and (b) demagnetizing field B_d of $(CoFeZr)_x(CaF_2)_{(100-x)}$ $(31$ at.% $\le x \le 47$ at.%$)$ films on CoFeZr concentration (x).

matrix. As discussed earlier, the behavior of $g(x)$ is explained by the presence of core-shell structure of NPs represented by ferromagnetic core and antiferromagnetic (ferrimagnetic) core which results in quenching of orbital motion of electrons.

The greater values of g-factor than samples with Al_2O_3 matrix also produced in Ar with O_2 sputtering atmosphere are explained by the less relative contribution of oxidized shell in the case of $(CoFeZr)_x(CaF_2)_{(100-x)}$ granular films.

Similarly, the greater values of g-factor observed for $(CoFeZr)_x(CaF_2)_{(100-x)}$ films than samples with Al_2O_3 matrix in the case of samples produced in Ar sputtering atmosphere can be explained by the greater average size of metal NPs [30].

The dependences of B_d on FeCoZr concentration x of two types of films are shown in Figure 5(b). It is seen that for the same FeCoZr concentration, granular films containing core-shell NPs are characterized with much lower values of B_d those for the films with pure FeCo-base NPs. As far as B_d is proportional to the value of films magnetization, such a decrease is directly related to the core-shell structure of NPs when films are deposited in Ar with O_2 atmosphere. At the same time, observed increase of B_d with x indicated in Figure 5(b) both for non-oxidized and oxidized films is naturally explained by the growth of magnetization due to the growth of NPs contribution in Al_2O_3 matrix.

The values of B_d for $(CoFeZr)_x(CaF_2)_{(100-x)}$ films are less than that for $(CoFeZr)_x(Al_2O_3)_{(100-x)}$ samples for $x > 42$ at.% as represented in [23]. On one hand, this mismatch can be explained by different volume fractions of metal at the same values of metal content for samples with CaF_2 and Al_2O_3 matrixes. On the other hand, the parameter B_d was defined as $B_d = (N_{IP} — N_{OOP}) \cdot \mu_0 \cdot M$, and the values magnetizations of metal NPs in different matrixes do not differ dramatically [20, 24, 27, 29]. We suppose that the decrease of B_d can also be caused by the presence of additional contribution to magnetic anisotropy associated with the elongated form of NPs in CaF_2 matrix as described in [20, 31]. However, the last assumption needs more detailed investigations.

4. CONCLUSIONS

Nanocomposites $(CoFeZr)_x(CaF_2)_{(100-x)}$ were produced by the ion sputtering method of a FeCoZr alloy target with CaF_2 dielectric strips attached to it. The content of the metallic phase ranged from 31 at.% to 47 at.%, i.e., below the percolation threshold $x_c \approx 50$ at.%. Two series of samples were prepared when films were sputtered in pure Ar and mixed Ar with O_2 atmospheres.

By means of transmission electron microscopy, it is found that in the first series, the dimensions of the metallic phase nanoparticles are in the range from about 1.5 nm to 6.5 nm. The dimensional distribution is similar to the Gaussian distribution with an average value of approx. 3.3 nm and a standard deviation of approx. 0.25 nm. In the second series, the nanoparticles have dimensions of about 6–8 nm. Electronographic studies have shown that nanoparticles from the first series of samples consist of the CoFeZr metallic phase. In contrast, nanoparticles in samples of the second series consist of metal oxides CoO and $Fe(Co)_xO_y$.

The magnetic properties of the nanocomposites $(CoFeZr)_x(CaF_2)_{(100-x)}$ with metallic phase content 31 at.% $\leq x \leq$ 47 at.% produced by ion-beam sputtering in Ar and Ar with O_2 atmosphere were analyzed on the basis of angular dependencies of the induction of resonance field $B_r(\theta_B)$. Values of g-factor and B_d are determined considering values of B_r at two orientations $\theta_B = 0°$ and $\theta_B = 90°$, and then, using these values, theoretical dependencies of $B_r(\theta_B)$ and $\theta_M(\theta_B)$ for the film $(CoFeZr)_{31}(CaF_2)_{69}$ were calculated. A good agreement of experimental data with theoretical calculation indicates an applicability of mathematic model. For Ar sputtering atmosphere, the value of g increases with the rise of metal content, and for Ar + O_2 atmosphere, this value decreases. The presence of core-shell structure of NPs results in quenching of orbital motion of electrons. Compared to nanocomposites $(CoFeZr)_x(Al_2O_3)_{(100-x)}$, the values of g are greater for examined materials and can be explained by the less relative contribution of oxidized shell for oxidized samples, and by the greater average size of metal NPs for non-oxidized samples. The lower values of B_d for $(CoFeZr)_x(CaF_2)_{(100-x)}$ than samples with Al_2O_3 matrix for $x > 42$ at.% were probably caused by additional contribution to magnetic anisotropy associated with the elongated form of NPs in CaF_2 matrix. As a conclusion, it can be argued that in nanocomposites $(CoFeZr)_x(CaF_2)_{(100-x)}$ the core-shall structure of NPs is formed, similar to the nanocomposites $(CoFeZr)_x(Al_2O_3)_{(100-x)}$.

ACKNOWLEDGMENT

REFERENCES

1. Pogrebnjak, A. D. and V. M. Beresnev, *Nanocoatings Nanosystems Nanotechnologies*, Bentham Science Publishers Ltd., 2012.

2. Pogrebnjak, A. D., V. M. Beresnev, K. V. Smyrnova, Y. O. Kravchenko, P. V. Zukowski, and G. G. Bondarenko, "The influence of nitrogen pressure on the fabrication of the two-phase superhard nanocomposite (TiZrNbAlYCr)N coatings," *Materials Letters*, Vol. 211, 316–318, 2018.

3. Pogrebnjak, A., V. Ivashchenko, O. Bondar, V. Beresnev, O. Sobol, K. Załęski, S. Jurga, E. Coy, P. Konarski, and B. Postolnyi, "Multilayered vacuum-arc nanocomposite TiN/ZrN coatings before and after annealing: Structure, properties, first-principles calculations," *Materials Characterization*, Vol. 134, 55–63, 2017.

4. Bayev, V., E. Streltsov, M. Milosavljević, M. Malashchonak, A.Maximenko, T. N. Koltunowicz, P. Zukowski, and K. Kierczyński, "Magnetic anisotropy in bicomponent self-assembled Ni and Ni-Pd nanowires studied by magnetic resonance spectroscopy," *IEEE Transactions on Magnetics*, Vol. 51, No. 10, 2300307, 2015.

5. Gubin, S. P., Y. A. Koksharov, G. B. Khomutov, and G. Y. Yurkov, "Magnetic nanoparticles: Preparation, structure and properties," *Russian Chemical Reviews*, Vol. 74, No. 6, 489–520, 2005.

6. Respaud, M., J. Broto, H. Rakoto, A. R. Fert, L. Thomas, B. Barbara, M. Verelst, E. Snoeck, P. Lecante, A. Mosset, J. Osuna, T. Ould Ely, C. Amiens, and B. Chaudret, "Surface effects on the magnetic properties of ultrafine cobalt particles," *Physical Review B — Condensed Matter and Materials Physics*, Vol. 57, No. 5, 2925–2935, 1998.

7. Partyka, J., P. Zukowski, P. Wegierek, M. Kowalski, Y. Sidorenko, V. Stelmakh, N. Lapchuk, and E. Shumskaya, "Magnetic properties of semiconducting compounds: $Cd_{1-x}Fe_xTe$ and $Cd_{1-x}Mn_xTe$," *Optoelectronic and Electronic Sensors V*, Editor, Proceedings of SPIE, Vol. 5124, 120–124, 2003.

8. Kumar, D., J. Narayan, A. V. Kvit, A. K. Sharma, and J. Sankar, "High coercivity and superparamagnetic behavior of nanocrystalline iron particles in alumina matrix," *Journal of Magnetism and Magnetic Materials*, Vol. 232, No. 3, 161–167, 2001.

9. Wang, C., Y. Rong, and T. Y. H. (Xu Zuyao), "Key role in giant magnetoresistance of granular films: Single-domain ferromagnetic granules," *Journal of Magnetism and Magnetic Materials*, Vol. 305, No. 2, 310–314, 2006.

10. Dempsey, N. M., L. Ranno, D. Givord, J. Gonzalo, R. Serna, G. T.Fei, A. K. Petford-Long, R. C. Doole, and D. E. Hole, "Magnetic behavior of $Fe:Al_2O_3$ nanocomposite films produced by pulsed laser deposition," *Journal of Applied Physics*, Vol. 90, No. 12, 6268–6274, 2001.

11. Zhu, T. and Y. J. Wang, "Enhanced tunneling magnetoresistance of (formula presented) granular films in the coulomb blockade regime," *Physical Review B — Condensed Matter and Materials Physics*, Vol. 60, No. 17, 11918–11921, 1999.

12. Mitani, S., S. Takahashi, K. Takanashi, K. Yakushiji, S.Maekawa, and H. Fujimori, "Enhanced magnetoresistance in insulating granular systems: Evidence for higher-order tunneling," *Physical Review Letters*, Vol. 81, No. 13, 2799–2802, 1998.

13. Judy, J. H., "Advancements in PMR thin-film media," *Journal of Magnetism and Magnetic Materials*, Vol. 287, 16–26, 2005.

14. Timopheev, A. A., S. M. Ryabchenko, V. M. Kalita, A. F. Lozenko, P. A. Trotsenko, O. V. Stognei, and A. V. Sitnikov, "Growth-induced perpendicular anisotropy of grains in Co-Al-O nanogranular ferromagnetic films," *Physics of the Solid State*, Vol. 53, No. 3, 494–503, 2011.

15. Ivanov, V. E., "Mixed magnetooptical contrast induced by an inhomogeneous magnetic field in metal films with planar anisotropy," *Technical Physics Letters*, Vol. 35, No. 5, 435–439, 2009.

16. Ivanov, V. E., "Visualization of nonuniform magnetic fields by gadolinium-cobalt amorphous films," *Physics of Metals and Metallography*, Vol. 105, No. 5, 453–459, 2008.

17. Kalinin, Y. E., A. T. Ponomarenko, A. V. Sitnikov, and O. V. Stognej, "Granular metal-insulator nanocomposites with amorphous structure," *Fizika i Khimiya Obrabotki Materialov*, No. 5, 14–20, 2001.

18. Zolotukhin, I. V., Y. U. E. Kalinin, A. T. Ponomarenko, V. G. Shevchenko, A. V. Sitnikov, O. V. Stognei, and O. Figovsky, "Metal-dielectric nanocomposites with amorphous structure," *Journal of Nanostructured Polymers and Nanocomposites*, Vol. 2, No. 1, 23–24, 2006.

19. Himpsel, F. J., J. E. Ortega, G. J. Mankey, and R. F. Willis, "Magnetic nanostructures," *Advances in Physics*, Vol. 47, No. 4, 511–597, 1998.

20. Kasiuk, J. V., J. A. Fedotova, J. Przewoznik, J. Zukrowski, M. Sikora, C. Kapusta, A. Grce, and M. Milosavljević, "Growth-induced non-planar magnetic anisotropy in FeCoZr-CaF$_2$ nanogranular films: Structural and magnetic characterization," *Journal of Applied Physics*, Vol. 116, No. 4, 044301, 2014.

21. Kasiuk, J. V., J. A. Fedotova, J. Przewoznik, C. Kapusta, M. Sikora, J. Zukrowski, A. Grce, and M. Milosavljević, "Oxidation controlled phase composition of FeCo(Zr) nanoparticles in CaF$_2$ matrix," *Materials Characterization*, Vol. 113, 71, 2016.

22. Weil, J. A. and J. R. Bolton, *Electron Paramagnetic Resonance: Elementary Theory and Practical Applications*, 592, Wiley, New York, 1994.

23. Kołtunowicz, T. N., P. Zukowski, J. Sidorenko, V. Bayev, J. A. Fedotova, M. Opielak, and A. Marczuk, "Ferromagnetic resonance spectroscopy of CoFeZr-Al$_2$O$_3$ granular films containing 'FeCo core — oxide shell' nanoparticles," *Journal of Magnetism and Magnetic Materials*, Vol. 421, 98–102, 2017.

24. Saad, A. M., A. K. Fedotov, J. A. Fedotova, I. A. Svito, B. V. Andrievsky, Y. E. Kalinin, V. V. Fedotova, V. Malyutina-Bronskaya, A. A. Patryn, A. V. Mazanik, and A. V. Sitnikov, "Characterization of $(Co_{0.45}Fe_{0.45}Zr_{0.10})_x(Al_2O_3)_{1-x}$ nanocomposite films applicable as spintronic materials," *Physica Status Solidi C – Current Topics in Solid State Physics*, Vol. 3, No. 5, 1283, 2006.

25. Fedotova, J. A., J. Przewoznik, C. Kapusta, M. Milosavljevic, J. V. Kasiuk, J. Zukrowski, M. Sikora, A. A. Maximenko, D. Szepietowska, and K. P. Homewood, "Magnetoresistance in FeCoZr-Al$_2$O$_3$ nanocomposite films containing metal coreoxide shell nanogranules," *Journal of Physics D: Applied Physics*, Vol. 44, No. 49, 495001, 2011.

26. Fedotova, J. A., "Tailored magnetic and electric states in 3d-metal-insulator films: Characterization and applications," *Acta Physica Polonica A*, Vol. 125, No. 4, 944–952, 2014.

27. Fedotova, J., J. Kasiuk, J. Przewoznik, C. Kapusta, I. Svito, Y. Kalinin, and A. Sitnikov, "Effect of oxide shells on the magnetic and magnetotransport characteristics of oxidized FeCoZr nanogranules in Al$_2$O$_3$," *Journal of Alloys and Compounds*, Vol. 509, No. 41, 9869–9875, 2011.

28. Cullity, B. D. and C. D. Graham, *Introduction to Magnetic Materials*, 544, John Wiley & Sons, Inc., Hoboken, New Jersey, 2008.

29. Landau, L. D. and E. M. Lifshitz, *Electrodynamics of Continuous Media (Second Edition Revised and Enlarged)*, Pergamon, Amsterdam, 1984.

30. Nibarger, J. P., R. Lopusnik, Z. Celinski, and T. J. Silva, "Variation of magnetization and the Landé g factor with thickness in Ni-Fe films," *Applied Physics Letters*, Vol. 83, No. 1, 93–95, 2003.

31. Vyzulin, S. A., E. V. Lebedeva, A. V. Maksimochkina, N. S. Perov, N. E. Syr'ev, and I. T. Trofimenko, "Peculiarities of the ferromagnetic resonance in multilayer CoFeZr-α-Si films," *Bulletin of the Russian Academy of Sciences: Physics*, Vol. 71, No. 5, 673–676, 2007.